7430 *Macromolecules* **2009**, *42*, 7430–7438
DOI: 10.1021/ma9015032

Macromolecules
ARTICLE

A New Approach to Polymer Self-assembly into Stable Nanoparticles: Poly(ethylacrylic acid) Homopolymers

Marián Sedlák*,[†] and Čestmír Koňák[‡]

[†]*Institute of Experimental Physics, Slovak Academy of Sciences, Watsonova 47, 040 01 Košice, Slovakia, and* [‡]*Institute of Macromolecular Chemistry, Academy of Sciences of the Czech Republic, Heyrovsky Sq. 2, 162 06 Prague 6, Czech Republic*

Received May 7, 2009; Revised Manuscript Received August 12, 2009

ABSTRACT: A new approach to polymer self-assembly is presented where stable polymeric nanoparticles are formed from homopolymers of one type only and without any assembly triggering additives. The mechanism of the self-assembly is based on the following idea. A thermosensitive polymer solution is heated, the solvent quality gradually worsen upon heating and polymer−polymer contacts are preferred over polymer−solvent contacts, which leads to the formation of polymer assemblies. Upon subsequent cooling to laboratory temperature, the assemblies should eventually dissolve, however, this is not the case due to the fact that polymer chains brought to a close proximity at elevated temperatures become hydrogen-bonded. In addition, hydrogen bonds strengthen upon cooling. As a result, stable nanoparticles are obtained. This mechanism is illustrated on poly(ethylacrylic acid) (PEA) homopolymers, which create a thermoresponsive system at certain degrees of ionization. Nanoparticles are resistant to agglomeration and macroscopic phase separation during heating as well as upon cooling down. The size of nanoparticles can be monitored during the growth and custom-tailored by tuning critical parameters, especially the temperature and time of heating. Nanoparticles are stable over long periods of time. They are stable in a broad range of salt concentrations, including physiological conditions, and possess a mild acceptable degree of polydispersity. Investigation of PEA solution properties, monitoring of the self-assembly process as well as a detailed characterization of nanoparticles were performed by static, dynamic, and electrophoretic light scattering. A comparison with the most related polymers (poly(methacrylic acid) and poly(propylacrylic acid)) was also performed.

Introduction

Polymeric nanoparticles of various nature are being developed and investigated because of numerous existing or foreseen applications. These are medical diagnostics, paints, coatings in the form of adsorbed layers and films of particles, photonic crystals, fillers for composite materials, etc. Carriers for targeted drug delivery represent currently perhaps the most important application. Polymeric nanoparticles are prepared either by chemical reactions (covalent bonds, e.g., latexes, microgels) or by various types of self-assembly (physical bonds). The self-assembly by physical forces is based on the whole variety of mechanisms, e.g., copolymer self-assembly in selective solvents (hydrophobic interaction of less soluble blocks),[1−6] association of ionic homopolymers with opposite charges due to electrostatic attraction,[7−10] association of two or more types of homopolymers due to intermolecular hydrogen bonding,[11−14] association of (co)polymers triggered by surfactants,[15,16] termination of the homopolymer phase separation by surfactants which stabilize the system in a dispersed state,[17,18] etc.

We describe in this work a new approach to polymer self-assembly into stable polymeric nanoparticles by introducing a mechanism where (i) polymeric nanoparticles are formed from homopolymers of one type only and (ii) the self-assembly is not triggered by any additives. The mechanism of the self-assembly is based on the following idea. A thermosensitive polymer solution is heated, polymer−polymer contacts are preferred over polymer−solvent contacts due to the worsening of the solvent quality, which leads to the formation of polymer assemblies. Upon subsequent cooling to laboratory temperature, the assemblies should eventually dissolve; however, this is not the case due to the fact that polymer chains brought to a close proximity at elevated temperatures become hydrogen-bonded. In addition, hydrogen bonds strengthen upon cooling. As a result, stable nanoparticles are obtained. An important assumption is that nanoparticles are resistant to agglomeration and macrophase separation during heating as well upon cooling to ambient temperature. The preparation of nanoparticles by this mechanism was motivated by our older results[19] on effects of heat-induced irreversible aggregation of poly(methacrylic acid), which was rather weak for utilization in the design of nanoparticles, but was fully irreversible.

Results on the successful preparation of nanoparticles based on poly(ethylacrylic acid) (PEA) homopolymers are presented in the current series (this work and accompanying paper[20]). The first paper of this series comprises of a detailed description of the self-assembly process and resulting product in terms of structural characteristics and is based mainly on light scattering methods (static, dynamic, and electrophoretic). It also contributes to the better understanding of solution properties of PEA, which were studied so far scarcely unlike solution properties of very common polycarboxylic polymers, poly(acrylic acid) (PAA) and poly(methacrylic acid) (PMA). A brief comparison of results on polymer association in a series of PMA, PEA and PPA (poly(propylacrylic acid)) is also covered in the first paper. The second paper[20] brings a deeper insight into of the self-assembly process by a combination of light scattering methods with calorimetry, FTIR spectroscopy, and quantum chemical calculations. The above-mentioned mechanism is potentially applicable also to other polymers provided they fulfill certain requirements.

*Corresponding author. E-mail: marsed@saske.sk.

 Published on Web 09/08/2009

Experimental Section

Material. Poly(ethylacrylic acid), $M_w = 18\,600$, $M_n = 12\,400$, $M_w/M_n = 1.5$, and poly(propylacrylic acid), $M_w = 47\,000$, $M_n = 22\,400$, $M_w/M_n = 2.1$, were obtained from Polymer Source, Canada, and used as delivered. PMA, $M_w = 70\,000$, was prepared by radical polymerization. The moisture content in the bulk polymer was established by Karl Fischer method and taken into account in the preparation of exact concentrations. Low molar mass substances were of analytical grade (Merck, Darmstadt, Germany). Water was freshly double-distilled in a quartz apparatus and subsequently deionized by analytical grade mixed-bed ion exchange resins (Bio-Rad, Richmond, CA). The resistivity of water was above 15 MΩ cm.

Static Light Scattering. The static light scattering (SLS) as well as dynamic light scattering (DLS) measurements were made using a Stabilite 2017−04S argon laser (Spectra Physics, Mountain View, CA) with 514.5 nm vertically polarized beam. Laser power was limited to 100 mW maximum via neutral density filters. A laboratory made goniometer with angular range from 30° to 150° was used to collect data for both static and dynamic light scattering experiments. The scattering cell was thermostated at 25 °C with a precision of ± 0.1 °C. All solutions were filtered through 0.2 μm filters. Scattering intensities were measured by photon counting. Solvent scattering was subtracted from total solution scattering to obtain excess scattering intensity. A distilled benzene standard was used for the scattering intensity normalization. Scattering intensities are normalized throughout the work as ratios I/I_B where I_B is benzene scattering. For the determination of absolute values of molecular weight M_w via a Zimm plot, Rayleigh ratios R_θ were calculated also using a benzene standard. Molecular weight M_w of nanoparticles was calculated from a Zimm plot as

$$\lim_{\substack{c \to 0 \\ \theta \to 0}} \frac{Kc}{R_\theta} = \frac{1}{M_w} \tag{1}$$

where c is polymer concentration, R_θ is the Rayleigh ratio at scattering angle θ, and constant K is defined for vertically polarized incident light as

$$K = \frac{4\pi^2 n^2 (\mathrm{d}n/\mathrm{d}C)^2}{{\lambda_0}^4 N_A} \tag{2}$$

where N_A is Avogadro's number, λ_0 is the light wavelength in vacuum, n is solution refractive index, and $\mathrm{d}n/\mathrm{d}c$ is the refractive index increment. Radius of gyration R_g of nanoparticles can be obtained from the initial slope of the angular dependence at the $c \to 0$ extrapolation

$$\lim_{c \to 0} \frac{Kc}{R_\theta} = \frac{1}{M_w} + \frac{1}{3}\frac{{R_g}^2}{M_w} q^2 \tag{3}$$

or alternatively from a Guinier plot (plotting log R_θ against q^2), where q is the absolute value of scattering vector $q = (4\pi n/\lambda_0)\sin(\theta/2)$.

Dynamic Light Scattering. An ALV-5000/E correlator with a fast correlation board option (ALV, Langen, Germany) was used for photon correlation measurements. Characteristic decay times of dynamic modes τ_i and their relative amplitudes $A_i(\tau_i)$ were evaluated through the moments of distribution functions of decay times $A(\tau)$ obtained by fitting correlation curves using CONTIN[21] and GENDIST[22,23] programs as

$$g^{(1)}(t) = \int_0^\infty A(\tau) \mathrm{e}^{-t/\tau}\, \mathrm{d}\tau \tag{4}$$

Diffusion coefficients were calculated as $D_i = (1/\tau_i)q^{-2}$.

Polydispersity index PDI reflecting the size polydispersity of nanoparticles was obtained from the cumulant analysis of correlation curves. Fits had the form

$$\ln g^{(1)}(t) = \ln A - \overline{\Gamma} t + \frac{\mu_2}{2} t^2 - \frac{\mu_3}{6} t^3 \tag{5}$$

where $g^{(1)}(t)$ is the normalized field autocorrelation function, A is amplitude, $\overline{\Gamma}$ is the mean frequency, and μ_2 and μ_3 are the second and the third moments (cumulants), respectively. Polydispersity index PDI was calculated as PDI = $\mu_2/\overline{\Gamma}^2$. The physical meaning of PDI can be explained by assuming a Gaussian distribution of sizes R of nanoparticles in the form

$$f(R) = \frac{1}{\sigma\sqrt{2\pi}} \exp\left(-\frac{(R-\overline{R})^2}{2\sigma^2}\right) \tag{6}$$

where σ is the standard deviation

$$\sigma = \left(\overline{(R-\overline{R})^2}\right)^{1/2}$$

Then the PDI obtained from the cumulant fit equals PDI = $(\sigma/\overline{R})^2$. The Gaussian distribution has a typical bell shape with the two inflection points at $\overline{R} - \sigma$ and $\overline{R} + \sigma$, respectively. The distribution width characterized as the distance between the two inflection points equals 2σ . This quantity must not be confused with the *full width at half-maximum*. The "2σ width" corresponds not to the width at half of the maximum but at 1/1.65 of the maximum and is therefore slightly smaller.

Differential Refractometry. Refractive index increment $\mathrm{d}n/\mathrm{d}c$ was measured via DNDC-2010 differential refractometer from WGE Dr. Bures (Germany) operating on the principle of a double bending of a light beam upon passage from solvent to solution and back. The 535 nm wavelength was used. Since light scattering was measured at 514.5 nm, the error was negligible. The typical noise level was very small, less than 5×10^{-9} RIU. The main source of error emerging in measuring $\mathrm{d}n/\mathrm{d}c$ comes from the fact that, very rigorously speaking, $\mathrm{d}n/\mathrm{d}c$ of polyelectrolytes or polyelectrolyte nanoparticles should be measured after equilibrium dialysis against solvent. This step is usually skipped in practice since its time consumption and the problem with a possible change of solution concentration upon dialysis. The resulting error due to omission of equilibrium dialysis depends on the nature of salt used as a supporting electrolyte, more exactly on the nature of the co-ion since the error is due to a negative co-ion adsorption. In the case of NaCl used in this work, the true M_w of nanoparticles may be higher by few percent than the calculated value based on $\mathrm{d}n/\mathrm{d}c$ measured without dialysis. The calculation based on semiempirical formulas for linear polyelectrolyte coils[24,25] yields for our polymer charge density and NaCl salt a 10% difference between calculated and true values of M_w, respectively. A smaller difference is anticipated for nanoparticles, which are denser compared to polymer coils.

Electrophoretic Light Scattering. Zeta potential of nanoparticles was obtained via BIC Zeta PALS analyzer (Brookhaven Instruments, New York) using a principle of phase analysis of light scattered from a solution of particles under electric field. The instrument is equipped with a solid state laser with 28 mW output at 658 nm. The ζ potential in millivolt units was calculated from the electrophoretic mobility [μm cm (V s)$^{-1}$], which is a directly measured quantity in an ELS experiment, via the Smoluchowski model. The ζ potential was measured at least 10 times to check for repeatability.

Results and Discussion

Poly(ethylacrylic acid) (PEA) was well soluble in methanol. A complete solubility on a molecular level was easily checked by light scattering, which is extremely sensitive to any types of aggregation, residues of undissolved polymer material, and preexisting cross-linked aggregates in the dry polymer bulk material. In water, PEA was insoluble. Upon subsequent addition of NaOH, polymer became eventually soluble, however, a substantial NaOH addition was necessary to achieve solubility within

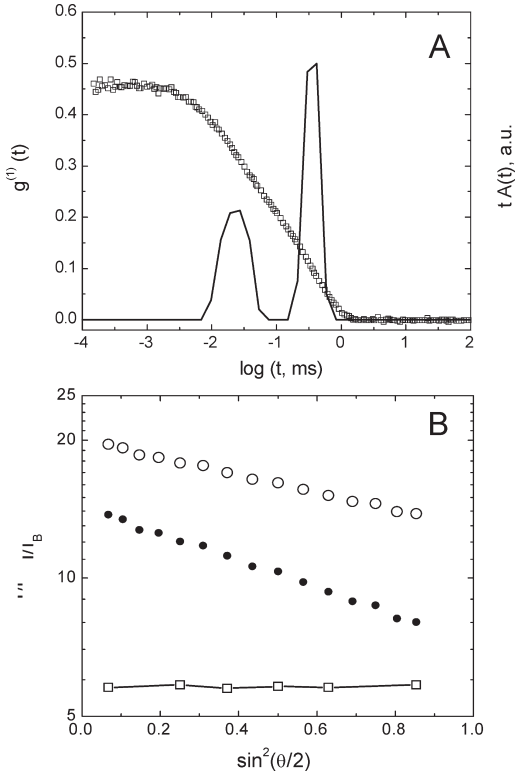

Figure 1. (A) Typical example of dynamic light scattering data from a solution of PEA in water partially ionized with NaOH. $\alpha = 0.21$, $c = 16$ g/kg, $c_s = 127$ mM NaCl. Field autocorrelation function $g^{(1)}(t)$ as well as the spectrum of relaxation times $A(t)$ are bimodal. The two diffusive modes are referred to as the fast and slow, respectively, and are characteristic of polyelectrolyte solution behavior. Scattering angle $\theta = 90°$. (B) Corresponding static light scattering data showing the total scattering (○) and scattering contributions from the fast (□) and slow (●) mode, respectively. Intensities shown are excess intensities (solvent contribution subtracted) and are normalized to benzene scattering I_B.

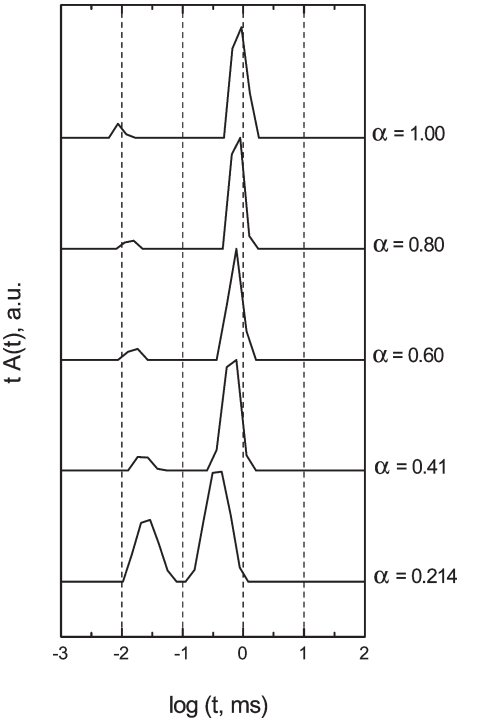

Figure 2. Spectra of relaxation times obtained from dynamic light scattering experiments on aqueous PEA solutions. Solution with $c = 20$ g/kg and degree of neutralization $\alpha = 1.0$ was prepared first by neutralization with NaOH and subsequently α was decreased by HCl addition. Scattering angle $\theta = 90°$.

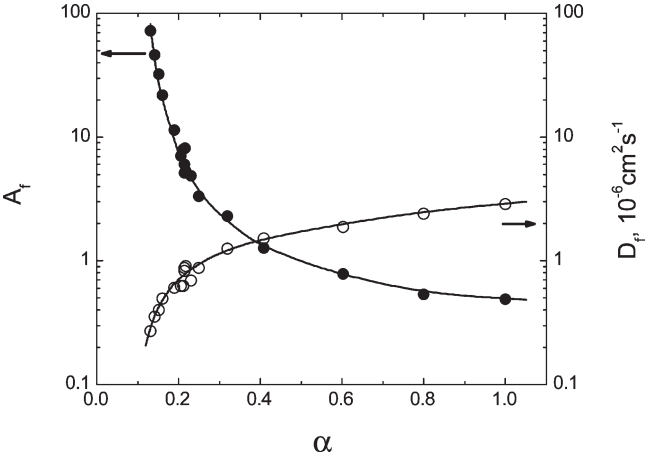

Figure 3. Dependence of the coupled mode diffusion coefficient D_f and corresponding scattering amplitude A_f on the degree of neutralization α. The same parameters as in Figure 2 were used.

acceptable times of stirring. Therefore, our approach was opposite. Polymer was first dissolved at the degree of neutralization $\alpha = 1.0$ ($\alpha = 1.0$ means full neutralization, i.e. equal molar concentrations of NaOH and PEA monomer). α was then decreased via back-titration by HCl. A typical polyelectrolyte behavior was seen in light scattering experiments. Figure 1 shows two dynamic modes, corresponding to the coupled diffusion of polyions and counterions (fast mode)[26−29] and diffusion of multimacroion domains (slow mode),[30−34] respectively. Angular dependencies of corresponding mode amplitudes A_f, A_s are shown in Figure 1B. The angular dependence of A_s arises from the fact that the size of multimacroion domains is comparable to the inverse scattering vector q^{-1} while individual polyions are small compared to q^{-1}. Diffusion coefficients are marked as D_f and D_s, respectively. Figure 2 shows the development of spectra of relaxation times upon decreasing the degree of neutralization α. The fast mode becomes slower, the slow mode becomes faster, and the A_s/A_f ratio decreases. This is expected on the basis of literature data on similar polyelectrolytes.[28,30,35] While numerous our papers were devoted to the slow mode behavior in the past, we will not focus on this subject in this work. The behavior of the fast mode is more relevant to the current topic. Figure 3 shows dependencies of A_f and D_f on the degree of neutralization α. An increase of the fast mode amplitude is evident upon decreasing α. This is mainly due to increased osmotic compressibility and is in agreement with results of previous works on similar polyelectrolytes: poly(methacrylic acid)[30] and poly(acrylic acid).[35] The influence of approaching the critical behavior upon lowering α is also possible (intensity increase by critical fluctuations or by formation of precritical aggregates). However, it is difficult to clearly separate these effects and it is also not a main topic of this work. Nevertheless, the tendency toward diverging of scattering intensity is clear. Diffusion coefficient exhibits just opposite behavior, which is also in agreement with the influence of an electrostatic effect (decreasing of polyion charge causes a decrease of diffusion coefficient similarly to other poly(carboxylic acids)[30,35]) and with the influence of approaching the critical temperature by lowering α. Another minor effect which comes into play in both the intensity and diffusion coefficient dependencies is due to the method of the sample preparation. Upon lowering α by HCl addition, a supporting electrolyte (NaCl) appears in solution with gradually increasing concentration. The effect of low molecular weight electrolyte (salt) results in increasing the intensity

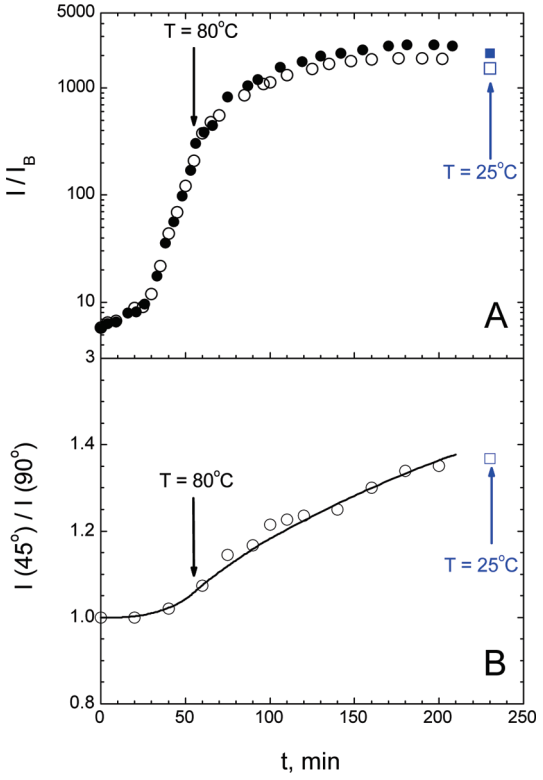

Figure 4. (A) Scattering intensity from a PEA solution, α = 0.21, c = 16 g/kg, c_s = 127 mM NaCl, during and after heating. Solution was heated from T = 25 °C to T = 80 °C at the heating rate 1 °C/min. Scattering angles: 90° (○) and 45° (●), respectively. Scattering after cooling down to T = 25 °C is also shown at angles 90° (□) and 45° (■), respectively. A dramatic increase is due to the irreversible formation of polymeric nanoparticles. (B) Ratio of scattering intensities at 45° and 90°, respectively. This reflects an increase of the radius of gyration of nanoparticles.

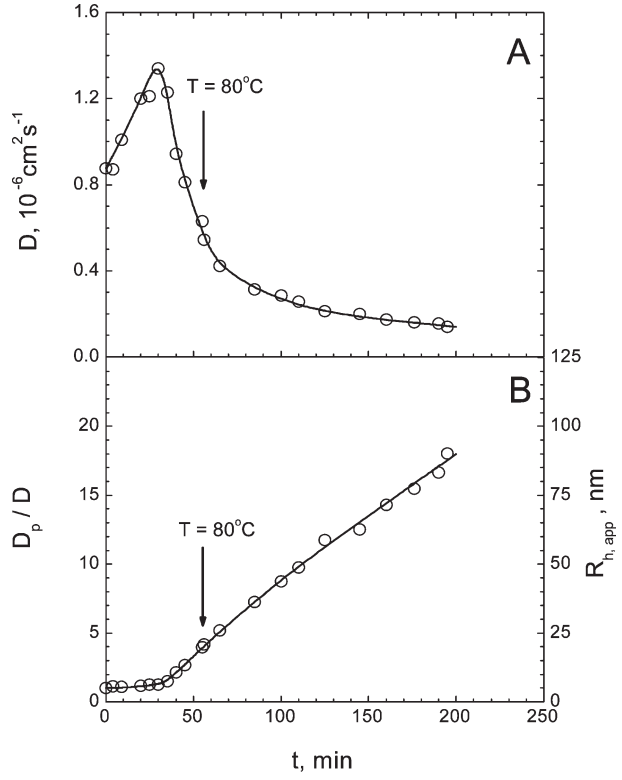

Figure 5. Time dependence of parameters from DLS during heating. Data refer to the sample from Figure 4: (A) diffusion coefficient; (B) ratio D_p/D, where D_p is the diffusion coefficient expected at temperature T provided that no change occurs in the sample upon heating except changes of T and solution viscosity η. Increase of D_p/D is due to the increase of the apparent hydrodynamic radius $R_{h,app}$ of nanoparticles.

and decreasing the diffusion coefficient due to shielding of electrostatic interactions and decoupling of polyion and counterion dynamics.[26−29] Upon further decrease of α, a macroscopic phase separation occurs at α ≅ 0.12.

The region near the phase separation (α ≅ 0.13−0.23, with corresponding pH values pH ≅ 5.2−5.8) is supposed to be associated also with intramolecular conformational changes of individual PEA chains. SAXS measurements on PEA solutions[36] showed that by decreasing α down to α = 0.2 the PEA conformation changes from wormlike to a more compact, with segment density higher than that in a wormlike chain but lower than that in a hard sphere. Conformational changes of individual chains are, however, not reflected in light scattering data due to a different q-range. Conformational changes of PEA chains in a similar pH range were reported by potentiometric titration[36−39] and fluorescence measurements.[40] These PEA properties were utilized later in the drug delivery oriented research, where PEA was used as a pH-sensitive membrane-disruptive agent incorporated in vesicles, liposomes or endosomes.[41−45]

It showed up as optimal for nanoparticle preparation to start with a PEA solution back-titrated from α = 1.0 to α = 0.21, with final polymer concentration c = 16 g/kg and concentration of supporting electrolyte (NaCl) c_s = 127 mM. This solution was heated to 80 °C at a rate 1 °C/min. Then the solution was kept at 80 °C for another 150 min. Figure 4A shows a dramatic increase of scattering intensity upon heating, which is due to polymer aggregation. Scattering intensity is normalized to benzene scattering.[50] After cooling down to 25 °C the intensity does not drop back, but remains constant due to the fact that polymer nanoparticles really do not dissolve, but remain stable.

The polymer aggregation accompanied by intensity increase continues also at the constant temperature of 80 °C. The gradual leveling off after ca. 100 min may be misleading. It does not mean that the process of the nanoparticle formation (growth) stops. It is due to an onset of multiple light scattering (MLS). MLS means that photons are multiply scattered on the sample while in regular scattering each photon interacts on average only once upon being detected by the detector. It is typical for the MLS regime that scattering intensity is constant or even decreases with increasing concentration and/or size of particles. Figure 4B shows the ratio of scattering intensities at scattering angles 45° and 90°, $I(45°)/I(90°)$, reflecting the increasing radius of gyration of nanoparticles R_g from static data. Figure 5A shows diffusion coefficient, which first increases upon heating, then sharply decreases. The initial increase is simply because of the increase of T/η. Then the nanoparticles start to form, grow in size, and cause a decrease of the diffusion coefficient due to the Stokes−Einstein relation $D = KT/6\pi\eta R_{h,app}$ (K is Boltzmann's constant, T is absolute temperature, η is viscosity, and $R_{h,app}$ is apparent hydrodynamic radius). An instructional plot is obtained upon correction for the change of T/η (Figure 5B). D_p/D is plotted here, where D is the actual measured diffusion coefficient at a given temperature T (from Figure 5A) and D_p is a "predicted diffusion coefficient" $D_p = D_{25}T\eta_{25}/T_{25}\eta$, where D_{25} is the diffusion coefficient measured at 25 °C (the reference temperature), η_{25} is viscosity at 25 °C and T_{25} = 298 K. Simply speaking, D_p is the diffusion coefficient expected at temperature T provided that nothing is changing in the sample upon heating except T and η. The deviation of D_p/D from unity is then a measure of the change of the apparent hydrodynamic radius. It is evident from Figure 5B that a continuous growth of nanoparticles begins ca. 30 min after the start of heating and continues until the end. The $R_{h,app}$ in

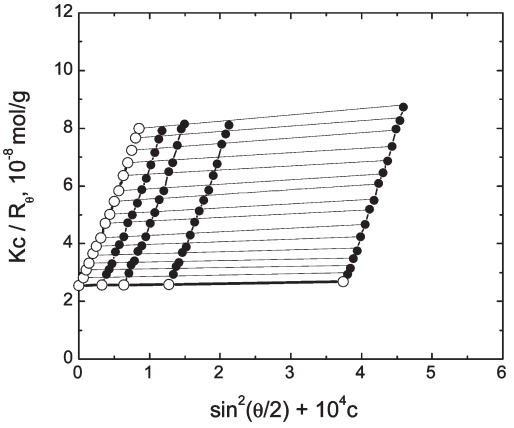

Figure 6. A Zimm plot for PEA nanoparticles in 127 mM NaCl. The intercept gives the molar mass of nanoparticles $M_w = 3.92 \times 10^7$ g/mol. The initial slope of the angular dependence at the $c \rightarrow 0$ extrapolation gives the radius of gyration $R_g = 81$ nm.

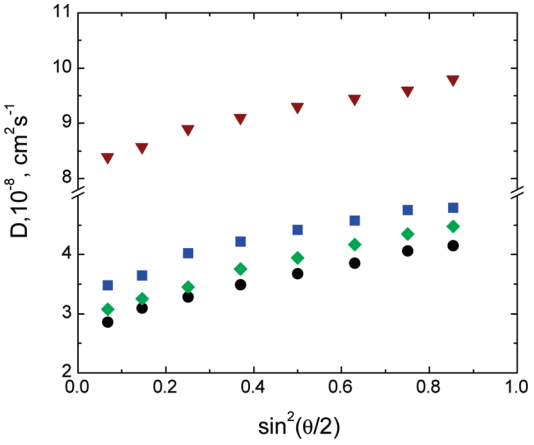

Figure 7. Angular dependence of diffusion coefficient of diluted PEA nanoparticles. Polymer concentration $c = 0.1$ g/kg. Concentration of supporting salt (NaCl) $c_s = 127$ mM. Different symbols correspond to different heating regimes used in the preparation process. See Figure 9 for more details.

Figure 5B is calculated only approximately since the initial $R_{h,app}$ at 25 °C is not known exactly.

An exact characterization of nanoparticles was done after cooling down and subsequent dilutions. First of all it is necessary to mention that the nanoparticles are resistant to dilution, i.e. that these are stable particles, not some equilibrium concentration-dependent associates. Figure 6 shows a typical Zimm plot. Refractive index increment dn/dc entering the relation Kc/R_θ in the Zimm plot was measured exactly at the conditions at which nanoparticles were formed, i.e. degree of neutralization $\alpha = 0.21$, and concentration of supporting salt $c_s = 127$ mM NaCl. The value dn/dc = 0.202 mL/g was measured. The double extrapolation of Kc/R_θ to zero scattering angle and concentration, respectively, yielded according to eq 1 the weight-average molecular weight of nanoparticles $M_w = 3.92 \times 10^7$ g/mol. The radius of gyration calculated from the Guinier plot at the $c \rightarrow 0$ extrapolation is $R_g = 81$ nm. The aggregation number (number of chains involved in a particle) is $N_a \sim 2100$.

Figure 7 shows DLS data on diluted nanoparticles. Diffusion coefficient is angularly dependent. The hydrodynamic radius calculated via Stokes−Einstein relation from the zero-angle extrapolated value $D(0°) = 2.8 \times 10^{-8}$ cm^2 s^{-1} is $R_h = 85.6$ nm. Solution viscosity $\eta = 0.905$ cP measured at $T = 25$ °C was used in the calculation. The angular dependence of diffusion coefficient may be due to two factors: (i) a consequence of the size polydispersity due to the relation $D_s \cong R_h^{-1}$ and (ii) the influence of internal dynamics. In the presence of internal dynamics of scatterers, the apparent diffusion coefficient can be expanded at low q as[51,52]

$$D(q) = D(0)(1+CR_g^2q^2-...) \quad \text{for } qR_g < 2 \qquad (7)$$

where C is a constant dependent on the internal architecture of the scattering particle (the C parameter is determined by the slowest internal mode of motion in the object) and values of C were reported[51,52] in the range from 0 to 0.2. Thus, for R_g comparable to q^{-1} (which is the case in this work), a measurable q-dependence of D can be obtained even for monodisperse particles. The contribution of the two effects (polydispersity and internal dynamics) cannot be easily separated. Since our nanoparticles do have a moderate degree of polydispersity (as deduced from the analysis of correlation curves) we anticipate mainly the influence of polydispersity on the angular dependence of D.

The ratio $R_g/R_h = 0.95$. Given the uncertainty in the estimate of corresponding radii and the polydispersity complication, we should instead write $R_g/R_h = 0.95 \pm 0.1$. Both R_g and R_h are z-averages, however, $R_{hz} \cong 1/\langle R_h^{-1}\rangle_z$ while

$$R_{gz} \cong \sqrt{\langle R_g^2\rangle_z}$$

and therefore large particles are more weighted in R_{gz}. Nevertheless the value $R_g/R_h = 0.95 \pm 0.1$ is reasonable for polymeric particles (assemblies). R_g/R_h values about 1.0 are predicted for random polycondensates (so-called soft balls) and star molecules.[53] R_g/R_h values about 1.0 were also found experimentally for polyelectrolyte complexes.[54] We remind that $R_g/R_h = 0.778$ is the theoretical value for homogeneous spheres and that in practice this ratio can deviate up or down according to the particle density, density distribution inside the particle, as well as to draining properties. Values clearly below 0.778, which are counterintuitive at first glance, were reported for microgels.[55,56] The apparent structural density ρ of PEA nanoparticles was calculated as an equivalent average density from M_w for the model of a sphere with the radius R_h, with no correction for polydispersity, $\rho = 3M_w/4\pi N_A R_h^3 = 0.025$ g/mL. The density of nanoparticles is smaller than those found for micelles in organic solvents ($\rho \approx 0.2$, see, e.g., ref 57) and for polyelectrolyte complexes ($\rho = 0.15-0.25$, see e.g. refs 58 and 59), but it is comparable with those found for branched structures. For instance, poly(vinyl acetate) exhibits values of ρ from $\rho = 0.001$ (branched polymer) to $\rho = 0.01$ (microgel) upon passing from pregel to postgel state inside particles, while at the same time R_g/R_h drops from 1.85 to 0.55.[55] The low density of nanoparticles under investigation is probably due to repulsive interactions between ionized carboxylic groups inside nanoparticles. As for the release of drugs, the low density can be advantageous since the sterical restrictions for a diffusion of low molecular molecules inside of particles are minimized.

Polydispersity index PDI of particle sizes R defined as PDI = $(\sigma/\overline{R})^2$, where σ is a standard deviation and also a halfwidth of the distribution, was obtained from dynamic light scattering by cumulant analysis as described in detail in the Experimental Section. PDI = 0.18 was obtained, which corresponds to a moderate polydispersity. Because of an inherent uncertainty arising from the ill-posed problem of fitting correlation curves in DLS and the noise level, even entirely monodisperse samples show a small degree of polydispersity. As a rule of thumb, samples with PDI ≤ 0.04 are considered monodisperse. The polydispersity of micelles[57] is usually smaller than 0.1 while that of polyelectrolyte complexes, e.g. DNA,[59] is in the range 0.1−0.2. Polydispersity of the most of latexes is above 0.1. Aggregates and

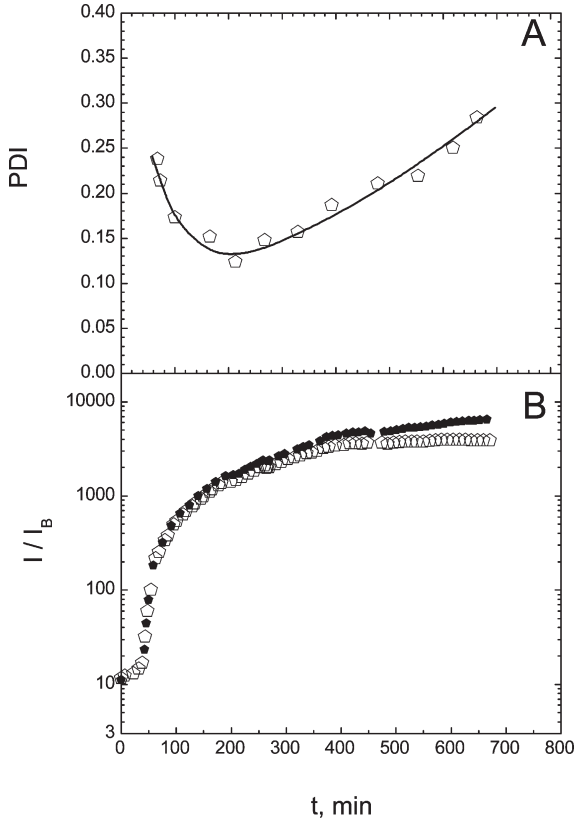

Figure 8. Development of polydispersity upon heating. PDI is a polydispersity index as determined from cumulant analysis. PEA solution, $\alpha = 0.225$, $c = 16$ g/kg, $c_s = 125$ mM NaCl, was heated from $T = 25$ °C to $T = 80$ °C at the heating rate 1 °C/min and then kept at $T = 80$ °C. Scattering angles were 90° (open symbols) and 45° (closed symbols), respectively.

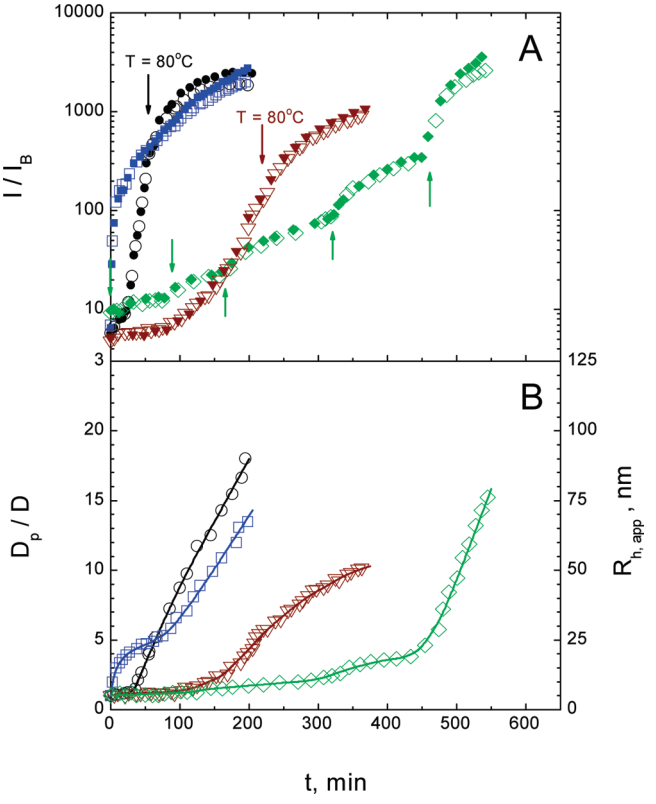

Figure 9. Effect of various heating regimes on the self-assembly behavior of PEA: (○) solution was heated from $T = 25$ °C to $T = 80$ °C at the heating rate 1 °C/min and then kept at $T = 80$ °C; (□) solution was placed directly into bath with $T = 80$ °C; (▽) solution was heated from $T = 25$ °C to $T = 80$ °C at the heating rate 0.25 °C/min and then kept at $T = 80$ °C; (◇) solution was heated stepwise to $T = 41$, 50, 60, 69, and 80 °C at the heating rate 1 °C/min. Arrows indicate beginning of each heating. The polymer concentration was $c = 16$ g/kg. Scattering angles: 90° (open symbols) and 45° (closed symbols), respectively.

microgels are also more polydisperse. The development of PDI with time of heating is shown in Figure 8. In the beginning, PDI as determined from cumulant analysis decreases toward a broad minimum around PDI ~ 0.13 accompanied by a slow increase of PDI upon further long heating. Smaller nanoparticles (terminated earlier) have thus smaller polydispersity. This is a rather typical behavior observed in aggregation processes.

Zeta potential of PEA nanoparticles was measured by the PALS method (phase analysis light scattering) as described in more details in the Experimental Section. A value of $\zeta = -36 \pm 2$ mV was measured, which means that nanoparticles are moderately charged. This ensures a good stability in aqueous environment. The negative charge is due to partially ionized carboxylic groups. The salt concentration, which otherwise influences ζ potentials, was during zeta potential measurements at the common value used in this work, i.e., $c_s = 127$ mM NaCl. More data on ζ will be covered in the next paper.

Effect of various heating regimes on the self-assembly behavior of PEA is documented in Figure 9. The rate of heating has no dramatic influence on the process. The main features remain the same, only small quantitative differences can be found. A stepwise heating of the solution was realized such that the sample was heated at a rate 1 °C/min to given temperature, then incubated at this temperature (partially equilibrated) and again heated at a rate 1 °C/min to a higher temperature, incubated, and so on.... It can be seen that the aggregation /self-assembly starts already somewhere at 40 °C although very weak and then gradually strengthens up to 80 °C. The transition is very broad, not occurring at a narrow interval of temperatures. This is in agreement with calorimetric data.[20] Using various heating regimes seems to have no dramatic practical value in terms of the control of the properties of resulting nanoparticles. Results on various heating regimes are though discussed in detail in the subsequent paper in relation to possible mechanisms of the stabilization of nanoparticles during heating (preventing from agglomeration and macroscopic phase separation).

The size of nanoparticles can be regulated simply by the time of incubation at $T = 80$ °C. The longer the time of incubation the larger particles can be obtained. Figure 10 summarizes results on the preparation of nanoparticles with varying size. The size (hydrodynamic radius) scales with molecular weight as $R_{h,app} \approx M_w^{0.50}$ (Figure 10A). A very similar scaling is also found for the radius of gyration (not shown). If we suppose the fractal character of the particles, then their size should scale as $R_{h,app} \approx M_w^{1/d_f}$ where d_f is the fractal dimension. In our case then $d_f = 1/0.50 = 2.0$. When the fractal grows, its density ρ should decrease unless $d_f = 3.0$. In general, ρ scales as $\rho \approx N_a^{(d_f-3)}/d_f$, where N_a is the aggregation number. Given $d_f = 2.0$ for our nanoparticles, ρ decreases as $\rho \approx M_w^{-1/2}$ (Figure 10C). The polydispersity index PDI increases with molecular weight (Figure 10B), which is quite typical for aggregation processes. PDI is mostly between 0.1 and 0.2, which is a moderate and acceptable degree of polydispersity of nanoparticles, nevertheless it slightly influences the above-mentioned scalings. $d_f = 2.0$ is predicted by percolation theory for fully swollen clusters,[60] however, a serious insight into the internal structure of nanoparticles as well as individual chains inside them is planned by SANS experiments.

Figure 11 shows long-time stability of PEA nanoparticles. Static and dynamic light scattering measurements were repeated after long time intervals (as long as one year) with practically

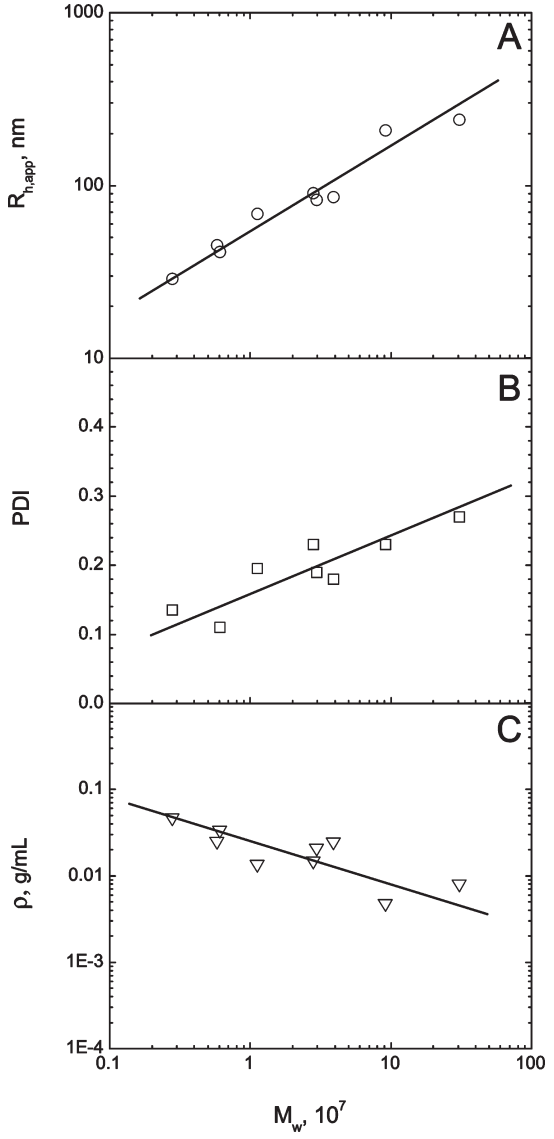

Figure 10. Molecular weight dependence of the hydrodynamic radius (○), polydispersity index (□), and density of PEA nanoparticles (▽).

identical results. Angular dependencies from SLS overlap as shown in Figure 11A. Values of diffusion coefficients (Figure 11B) also overlap within experimental accuracy. In conclusion, PEA nanoparticles are stable and do not change over long time intervals. Variation of the salt concentration in the range from 0.5 mM NaCl to 600 mM NaCl had no effect on the stability of nanoparticles. This means, of course, also stability at physiological salt concentration.

Figure 12 shows a summary of results obtained on the most related polymers to PEA: poly(methacrylic acid) (PMA) and poly(propylacrylic acid) (PPA). The most substantial difference between PMA and PEA is that the thermosensitivity of PMA is obtained only after suppressing the PMA ionization by addition of acid, e.g. HCl. The upper panel in Figure 12 shows the development of scattering intensity upon heating of PMA solutions. The heating rate was 1 °C/min, similarly to all data shown in Figure 12. At $\alpha = 0$ (not neutralized PMA), only a relatively small effect, i.e. a small increase of scattering intensity is seen upon heating to $T = 80$ °C. Further heating up to 95 °C does not lead either to a significant effect (not shown). The situation changes upon suppressing the weak natural ionization of PMA by HCl addition. Data on a PMA solution in 20 mM HCl are shown. Scattering intensity strongly increases and virtually

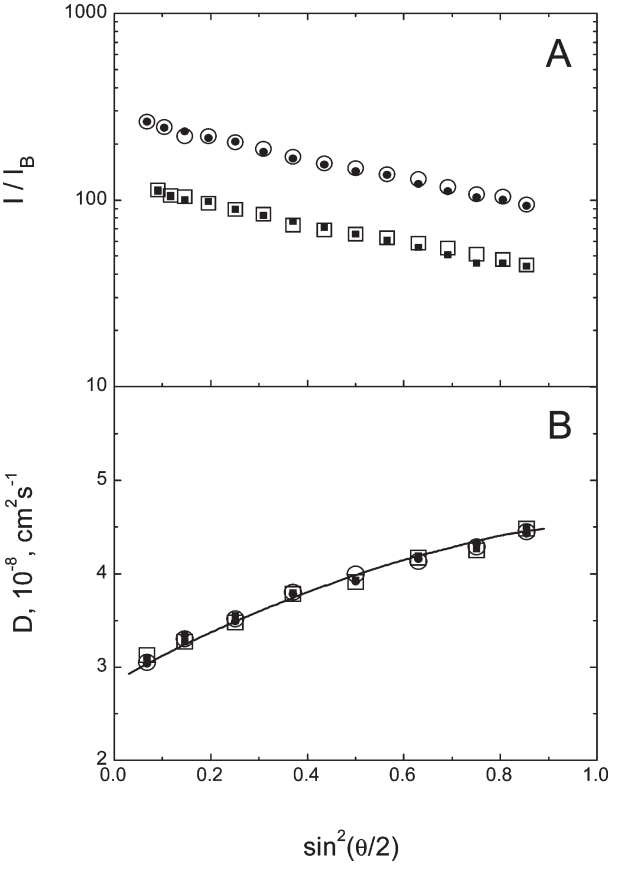

Figure 11. Long-time stability of PEA nanoparticles. Results from static and dynamic light scattering, respectively. Filled symbols: freshly prepared nanoparticles diluted to $c = 0.37$ g/kg (●) and $c = 0.13$ g/kg (■), respectively. Open symbols: the same solutions after two months (□) and 12 months (○), respectively.

diverges by approaching to $T = 71$ °C where a macroscopic phase separation occurs. This separation is reversible in a sense that the macroscopically segregated polymeric material dissolves upon decreasing temperature and solution becomes again optically transparent. However, a very thorough and detailed inspection by light scattering shows that some small traces of large polydisperse aggregates can be found in solution and persist weeks after cooling down (see blue symbols in Figure 12 as well as Figure 1 in the Supporting Information). In the case of solution with $\alpha = 0$, although the overall effect is very weak and no phase separation is observed, a careful inspection of solution after the heating cycle also shows some traces of very small aggregates, i.e. the overall scattering intensity does not drop exactly back to the original value. Nevertheless data from Figure 12 clearly show that PMA is not suitable for the preparation of nanoparticles by the presented method. Our observation of the phase separation at $T = 71$ °C in 20 mM HCl is in good agreement with literature data on the second virial coefficients yielding $A_2 = 0$ (Θ conditions) at $T = 56$ °C for PMA in 20 mM HCl.[47] In general, increasing the HCl concentration leads to decreasing the Θ temperature[48] as well as the phase separation temperature.

The behavior of PPA resembles more the behavior of PEA. Similarly to PEA, stable nanoparticles can be obtained by a fully irreversible heating cycle. Compared to PEA, the optimum conditions for their preparation shift to higher α values due to a shifted balance between the increased hydrophobicity of side groups promoting aggregation on one hand and the charge density promoting solubility on the other hand. However, in both cases (PEA and PPA) the thermosensitivity occurs in a regime of relatively strongly charged chains.

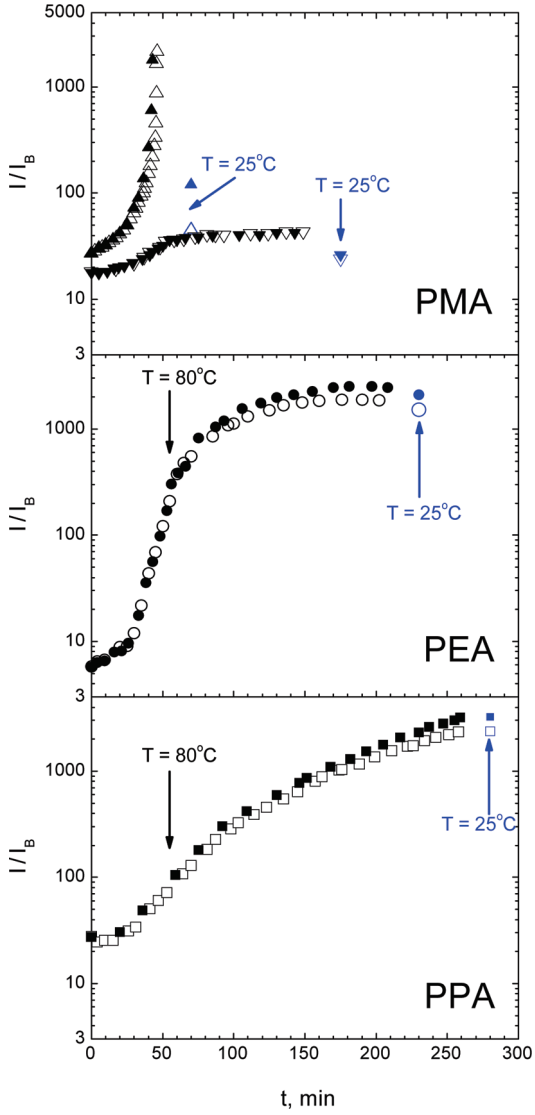

Figure 12. Comparison of behavior of PMA, PEA, and PPA upon heating. All solutions were heated from $T = 25$ °C to $T = 80$ °C at the same heating rate 1 °C/min. Benzene-normalized scattering intensities are shown at angles 90° (open symbols) and 45° (closed symbols), respectively. Scattering after cooling down to $T = 25$ °C is also shown (blue symbols). PMA: $c = 25$ g/kg, $\alpha = 0$ (∇) and in 20 mM HCl (Δ). PEA: $\alpha = 0.21$, $c = 16$ g/kg, PPA: $\alpha = 0.25$, $c = 16$ g/kg.

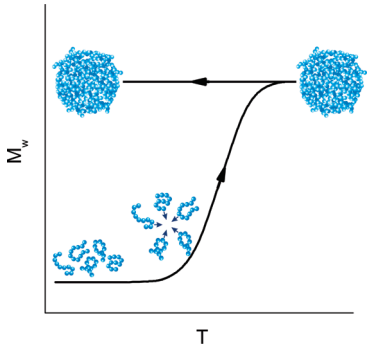

Figure 13. Schematic diagram of the self-assembly mechanism.

Conclusions

A new approach to polymer self-assembly was presented. Polymeric nanoparticles were prepared from homopolymers of one type only and without any assembly triggering additives. The self-assembly process was designed based on the following idea. A thermosensitive polymer solution is heated, the worsening of the solvent quality upon increasing temperature forces polymer chains to associate. At a close-enough distance, hydrogen bonds between chains become also operable and contribute to the stabilization of nanoparticles. The formation of hydrogen bonds in condensed particles will be discussed with a help of infrared spectroscopy and quantum chemical calculations in the subsequent paper.[20] As a result, nanoparticles do not dissolve upon cooling and remain stable. They are resistant to agglomeration during the heating process as well as after cooling down to ambient temperature. The self-assembly mechanism is schematically shown in Figure 13.

The size of PEA nanoparticles can be monitored during the growth and custom-tailored by tuning critical parameters, especially the temperature and time of heating. Obtained nanoparticles were stable over long periods of time. They are stable in a broad range of salt concentrations, including physiological conditions, and possess a mild acceptable degree of polydispersity. Moderate value of ζ potential $\zeta = -36$ mV assures good stability in aqueous solutions. The role of charges is also significant in preventing agglomeration and macroscopic phase separation. The next paper[20] provides a deeper insight into the mechanism of the self-assembly process and verifies the premises on which it was designed.

Acknowledgment. Support of the Research and Development Agency of the Slovak Republic (grant No. 51-037905), Slovak grant agency VEGA (Grant No. 2/6197/26), and Action COST D43 is acknowledged. Č.K. acknowledges support from the Grant Agency of the Czech Republic (Grant No. 202/09/2078). Authors are also thankful to E. Gyöngyösiová for technical assistance in experiments. This work was realized within the frame of the project "Centre of Excellence for Advanced Materials with Nano- and Submicron Structure", which is supported by the Operational Program "Research and Development" of the Slovak republic financed through European Regional Development Fund.

Supporting Information Available: Figure showing details of light scattering data after a temperature treatment cycle $T =$ 25 °C → 80 °C → 25 °C for PMA in 20 mM HCl. This material is available free of charge via the Internet at http://pubs.acs.org.

References and Notes

(1) Zhang, G.; Wu, C. *Adv. Polym. Sci.* **2006**, *195*, 101–176.
(2) Forster, S.; Antonietti, M. *Adv. Mater.* **1998**, *10*, 195–217.
(3) Allen, C.; Maysinger, D.; Eisenberg, A. *Colloids Surf. B: Biointerfaces* **1999**, *16*, 3–27.
(4) Riess, G. *Prog. Polym. Sci.* **2003**, *28*, 1107–1170.
(5) Lee, A. S.; Butun, V.; Vamvakaki, M.; Armes, S. P.; Pople, J. A.; Gast, A. P. *Macromolecules* **2002**, *35*, 8540–8551.
(6) Kataoka, K.; Harada, A.; Nagasaki, Y. *Adv. Drug Delivery Rev.* **2001**, *47*, 113–131.
(7) Dautzenberg, H. In *Physical Chemistry of Polyelectrolytes*; Radeva, T., Ed.; Marcel Dekker: New York, 2001; Chapter 20.
(8) Mattison, K. W.; Dubin, P. L. *J. Phys. Chem. B* **1998**, *102*, 3830–3836.
(9) Sui, Z. J.; Jaber, J. A.; Schlenoff, J. B. *Macromolecules* **2006**, *39*, 8145–8152.
(10) Schonhoff, M. *J. Phys.—Condens. Matter* **2003**, *15*, 1781–1808.
(11) Juang, M.; Li, M.; Xiang, M.; Zhou, H. *Adv. Polym. Sci.* **1999**, *146*, 121–196.
(12) Poe, G.; Jarrett, W.; Scales, C.; McCormick, C. *Macromolecules* **2004**, *37*, 2603–2612.
(13) Chen, H. L.; Morawetz, H. *Macromolecules* **1982**, *15*, 1445–1447.
(14) Sukhishvili, S. A.; Granick, S. *Macromolecules* **2002**, *35*, 301–310.
(15) Thunemann, A. F. *Prog. Polym. Sci.* **2002**, *27*, 1473–1572.
(16) Makhaeva, E. E.; Tenhu, H.; Khokhlov, A. R. *Macromolecules* **1998**, *31*, 6112–6118.

(17) Koňák, Č.; Hrubý, M. *Macromol. Rapid Commun.* **2006**, *27*, 877.
(18) Koňák, Č.; Pánek, J.; Hrubý, M. *Colloid Polym. Sci.* **2007**, *285*, 1433.
(19) Sedlák, M.; Koňák, Č.; Štěpánek, P.; Jakeš, J. *Polymer* **1990**, *31*, 253–257.
(20) Sedlák, M.; Koňák, Č.; Dybal, J. *in press*.
(21) Provencher, S. W. *Comput. Phys. Commun.* **1982**, *27*, 213–227.
(22) Jakeš, J. *Czech. J. Phys.* **1988**, *38*, 1305.
(23) Štěpánek, P. In *Dynamic Light Scattering. The Method and Some Applications* ; Clarendon: Oxford, U.K., 1993; Chapter 4.
(24) Sedlák, M. In *Light Scattering. Principles and Development*; Clarendon Press: Oxford, U.K., 1996; Chapter 4.
(25) Vrij, A.; Overbeek, J.; Th, G. *J. Colloid. Sci.* **1962**, *17*, 570–588.
(26) Lin, S. C.; Lee, W. I.; Schurr, J. M. *Biopolymers* **1978**, *17*, 1041.
(27) Schmitz, K. S. *Macroions in Solution and Colloidal Suspension*; VCH Publishers: New York, 1993.
(28) Sedlák, M. In *Physical Chemistry of Polyelectrolytes*; Marcel Dekker: New York, 2001; Chapter 1.
(29) Sedlák, M. *Langmuir* **1999**, *15*, 4045–4051.
(30) Sedlák, M.; Koňák, Č.; Štěpánek, P.; Jakeš, J. *Polymer* **1987**, *28*, 873–880.
(31) Schmitz, K. S.; Lu, M.; Gauntt, J. *J. Chem. Phys.* **1983**, *78*, 5059–5066.
(32) Fulmer, A. W.; Benbasat, J. A.; Bloomfield, V. A. *Biopolymers* **1981**, *20*, 1147–1159.
(33) Förster, S.; Schmidt, M.; Antonietti, M. *Polymer* **1990**, *31*, 781–792.
(34) Sedlák, M.; Amis, E. J. *J. Chem. Phys.* **1992**, *96*, 817–825.
(35) Sedlák, M. *J. Chem. Phys.* **2002**, *116*, 5256–5262.
(36) Muroga, Y.; Iida, S.; Shimizu, S.; Ikake, H.; Kurita, K. *Biophys. Chem.* **2004**, *110*, 49–58.
(37) Joyce, D. E.; Kurucsev, T. *Polymer* **1981**, *22*, 415–417.
(38) Fichtner, F.; Schönert, H. *Colloid Polym. Sci.* **1977**, 230–232.
(39) Sugai, S.; Nitta, K.; Ohno, N.; Nakano, N. *Colloid Polym. Sci.* **1983**, *261*, 159–165.
(40) Linhardt, J. G.; Thomas, J. L.; Tirrell, D. A. *Macromolecules* **1999**, *32*, 4457–4459.
(41) Linhardt, J. G.; Tirrell, D. A. *Langmuir* **2000**, *16*, 122–127.
(42) Jones, R. A.; Cheung, C. Y.; Black, F. E.; Zia, J. K.; Stayton, P. S.; Hoffman, A. S.; Wilson, M. R. *Biochem. J.* **2003**, *372*, 65–75.
(43) Kusonwiriyawong, C.; van de Wetering, P.; Hubbell, J. A.; Merkle, H. P.; Walter, E. *Eur. J. Pharm. Biopharm.* **2003**, *56*, 237–246.
(44) Hoffman, A. S.; Stayton, P. S.; Press, O.; Murthy, N.; Lackey, C. A.; Cheung, Ch.; Black, F.; Campbell, J.; Fausto, N.; Kyriakides, T. R.; Bornstein, P. *Polym. Adv. Technol.* **2002**, *13*, 992–999.
(45) El-Sayed, M. E. H.; Hoffman, A. S.; Stayton, P. S. *J. Controlled Release* **2005**, *104*, 417–427.
(46) Koňák, Č.; Sedlák, M. *Macromol. Chem. Phys.* **2007**, *208*, 1893–1899.
(47) Silberberg, A.; Elliassaf, J.; Katchalsky, A. *J. Polym. Sci.* **1957**, *23*, 259.
(48) Arnold, R.; Caplan, S. R. *Trans. Faraday Soc.* **1955**, *51*, 857.
(49) Eliassaf, J.; Silberberg, A. *Polymer* **1962**, *3*, 555.
(50) Intensity contribution from A_s is subtracted in Figure 4 since the intensity increase as shown by multimodal analysis is due to changes of the classical scattering A_f.
(51) Burchard, W.; Schmidt, M.; Stockmayer, W. H. *Macromolecules* **1980**, *13*, 580–587.
(52) Burchard, W.; Schmidt, M.; Stockmayer, W. H. *Macromolecules* **1980**, *13*, 1265–1272.
(53) Burchard, W. *Adv. Polym. Sci.* **1983**, *48*, 1.
(54) Oupický, D.; Koňák, Č.; Ulbrich, K. *J. Biomater. Sci., Polym. Ed.* **1999**, *10*, 573.
(55) Schmidt, M. In *Dynamic Light Scattering. The Method and Some Applications*; Clarendon: Oxford, U.K., 1993; Chapter 8.
(56) Burchard, W. In *Light Scattering. Principles and Development*; Clarendon Press: Oxford, U.K., 1996; Chapter 13.
(57) Tuzar, T.; Pleštil, J.; Koňák, Č.; Hlavatá, D.; Sikora, A. *Makromol. Chem.* **1983**, *184*, 2111–2121.
(58) Dautzenberg, H.; Koňák, Č.; Reschel, T.; Zintchenko, A.; Ulbrich, K. *Macromol. Biosci.* **2003**, *3*, 425.
(59) Reschel, T.; Koňák, Č.; Oupický, D.; Seymour, L. W.; Ulbrich, K. *J. Controlled Release* **2002**, *81*, 201.
(60) Stauffer, D. *Introduction to percolation theory*; Taylor & Francis: London, 1985.